npj | natural hazards

Article

https://doi.org/10.1038/s44304-025-00119-x

Rising compound hot-dry extremes engendering more inequality in human exposure risks

Check for updates

Junhong Guo[1,8], Feng Wang[2,8], Yizhuo Wen[3], Xiaoxuan Wang[1], Zhenda Hao[4], Heran Zheng[5], Yurui Fan[6] ✉ & Chunming Shen[7] ✉

Compound hot-dry events, with their amplified negative impacts on ecosystems and societies, are attracting growing attention. This study investigates the global-scale inequality and risks of hot-dry compound events under various shared socioeconomic pathways (SSP) scenarios, considering hazards, exposure, and vulnerability. Results show a worldwide increase in hot-dry extreme events and population exposure by mid-century (2041–2070), with variations among scenarios and regions. Climate factors are identified as the primary contributors to future changes in population exposure. SSP1-2.6 shows lower risks than SSP5-8.5 notably. Spatially, ASIA and the Middle East and Africa (MAF) will likely face higher exposure risks due to large populations, lower income levels and aging demographics, which amplify climate impacts. Under SSP3-7.0, rapid population growth introduces greater uncertainty in exposure estimates, particularly in ASIA, MAF, Latin America and the Caribbean (LAM). Aging populations, especially under SSP3-7.0 and SSP5-8.5 scenarios, exacerbate exposure risks through climate-demographic interactions.

Droughts and heat waves are among the most severe and frequent climate hazards globally, posing serious threats to both ecosystems and human societies[1]. Under global warming, high-temperature anomalies often coincide with prolonged precipitation deficits, giving rise to "hot-dry" events[2]. These events are driven not only by the thermodynamic relationship between temperature and precipitation but also by the influence of large-scale circulation patterns and land-atmospheric feedbacks[1,3,4]. Unlike isolated extreme events, compound hot-dry events intensify adverse impacts by simultaneously exerting pressure on both natural ecosystems and human systems. Beyond the immediate consequences of heatwaves and droughts, these extreme weather events can trigger cascading secondary crises, such as food insecurity[4,5], water scarcity[6], and an elevated risk of wildfires in forests and grasslands[7,8]. The increasing frequency and severity of such events have drawn growing attention in recent years[9–12].

Various definitions have been developed to identify hot-dry events, typically relying on either absolute thresholds or percentile-based criteria for temperature and precipitation anomalies[9]. Nevertheless, the utilization of absolute thresholds can underestimate the impacts of high temperatures in high latitude or historically cooler regions, where smaller anomalies may still have significant consequences[13]. Relative thresholds are thus often considered more suitable for global-scale and cross-regional assessments[14,15]. Moreover, heat extremes can also be characterized using daily mean temperature[16], minimum temperature[14], and perceived temperature[17]. For drought, precipitation serves as the primary indicator, supplemented by standardized metrics such as the Standardized Precipitation Index (SPI)[9,18] and the Standardized Precipitation Evapotranspiration Index (SPEI)[19], and soil moisture in some cases[20].

Current research on compound hot-dry events has made progress in characterizing their frequency, duration, and severity through historical observations, reanalysis datasets, and climate model projections[5,10,18,21,22]. Previous global-scale studies utilizing the Coupled Model Intercomparison Project Phase 5 and 6 (CMIP5 and CMIP6) simulations further suggest a substantial rise in compound hot-dry events under future climate scenarios[6,20,23–27]. To better capture the societal implications of these events,

[1]MOE Key Laboratory of Resource and Environmental System Optimization, College of Environmental Science and Engineering, North China Electric Power University, Beijing, China. [2]State Key Laboratory of Earth Surface Processes and Resource Ecology, Faculty of Geographical Science, Beijing Normal University, Beijing, China. [3]Key Laboratory of Environmental Biotechnology, Xiamen University of Technology, Xiamen, China. [4]Sustainability Standards Research Center, School of Economics, Central University of Finance and Economics, Beijing, China. [5]Sustainable Finance and Infrastructure Transition, Bartlett School of Sustainable Construction, University College London, London, UK. [6]Department of Civil and Environmental Engineering, Brunel University of London, Uxbridge, UK. [7]Beijing Academy of Science and Technology, Research Institute of Urban System Engineering, Beijing, China. [8]These authors contributed equally: Junhong Guo, Feng Wang. ✉e-mail: yurui.fan@brunel.ac.uk; Chunming_Shen@126.com

population exposure—defined as the number of people affected multiplied by the duration or intensity of extreme events—has emerged as a widely used metric for quantifying human risk and vulnerability[3,9,28].

Despite these advances, global-scale assessments of exposure inequalities related to compound extreme events remain limited. Few studies have incorporated vulnerability dimensions, such as income levels or aging populations, into global exposure assessments—even though these factors critically shape how risks are distributed across regions and demographic groups[29,30]. Another challenge lies in the climate data used to project future events. Global climate models differ in initial conditions, physical parameterizations, and resolutions, leading to uncertainty and potential biases in historical climate simulations, which may subsequently propagate into future projections[31]. Furthermore, the coarse spatial resolution of GCMs often limits their ability to capture local-scale climate signals and population heterogeneity[32]. This highlights the need for a high-resolution global climate dataset, appropriate downscaling and bias correction techniques to improve the accuracy of future projections[9,33].

Thus, this study aims to identify global hotspots and inequality patterns in exposure to compound hot-dry events under different climate and socioeconomic scenarios. We employ a bias-corrected, high-resolution GCM dataset to assess future changes in compound event hazards, exposure, and vulnerability across the globe under the SSP framework. Special attention is given to regional disparities in exposure, particularly with respect to population aging and income levels. The results are intended to support more targeted adaptation planning and international climate risk governance.

Results

Future changes in hot-dry extremes

As global temperature rises, there is an overall increasing trend in the frequency of hot-dry extreme events across most regions of the world, which is statistically significant at the 5% level (Fig. 1). Relative to the baseline period (1981–2010), significant changes in the annual mean duration of hot-dry events during the mid-century (2041–2070) are primarily concentrated in the low to mid-latitude regions near the equator. In particular, regions such as South America, Western and South Asia, the Middle East, and northern and central Africa are projected to experience notable increases in the number of hot-dry days. Under medium- to high-emission scenarios (i.e., SSP3-7.0 or SSP5-8.5), the annual average number of hot-dry days in these regions is expected to rise by more than 25 days compared to the baseline period. Additionally, under the SSP5-8.5 scenario, noticeable increases are projected in regions such as the eastern part of Greenland and central Australia. Although the spatial distribution of these changes remains generally consistent across different scenarios, both the frequency and spatial extent of hot-dry events are further amplified with increasing greenhouse gas concentrations, particularly under SSP5-8.5. To assess inter-model uncertainty, the 10th and 90th quantile results among GCM models are calculated. For the annual mean duration of hot-dry events (Fig. S1), greater uncertainty is observed near the equator and in the high-latitude regions of the Northern Hemisphere, particularly in areas such as northern South America, and central Africa.

Figure 2 illustrates the changes in the intensity of hot-dry compound extreme events during the mid-century period. With increasing greenhouse gas concentrations, the intensity of the hot component of compound events is expected to become more pronounced, accompanied by an expansion of affected areas (significant at the 5% level). Even under the low-emission SSP1-2.6, future hot event intensity is projected to increase by more than 1.0 K. Under SSP5-8.5, however, this increase could exceed 3.5 K. Spatially, the largest increases in hot intensity are concentrated around 45°N, notably in Asia, Europe, northern Africa, and North America. As emission levels increase, the spatial extent of hot event intensity expands into the Southern Hemisphere. On the other hand, although the dry intensity in hot-dry compound extreme events shows smaller changes across scenarios, it also

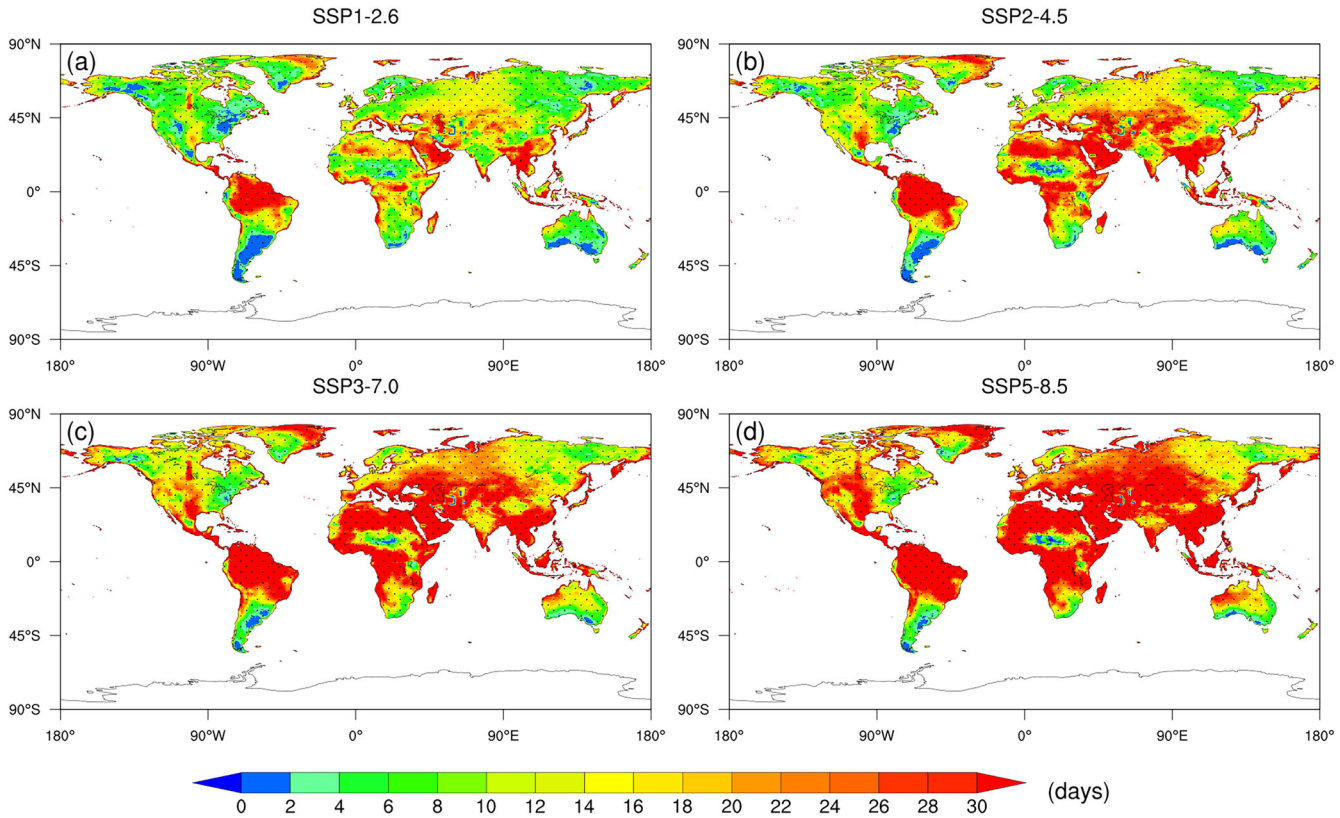

Fig. 1 | Projected changes in annual mean duration of hot-dry event under different SSP scenarios. Changes are shown for the period 2041–2070 relative to the baseline period (1981–2010): **a** SSP1-2.6, **b** SSP2-4.5, **c** SSP3-7.0, **d** SSP5-8.5. Light gray dots indicate areas where changes are statistically significant at a 5% level based on the Student's *t* test. (unit: days)

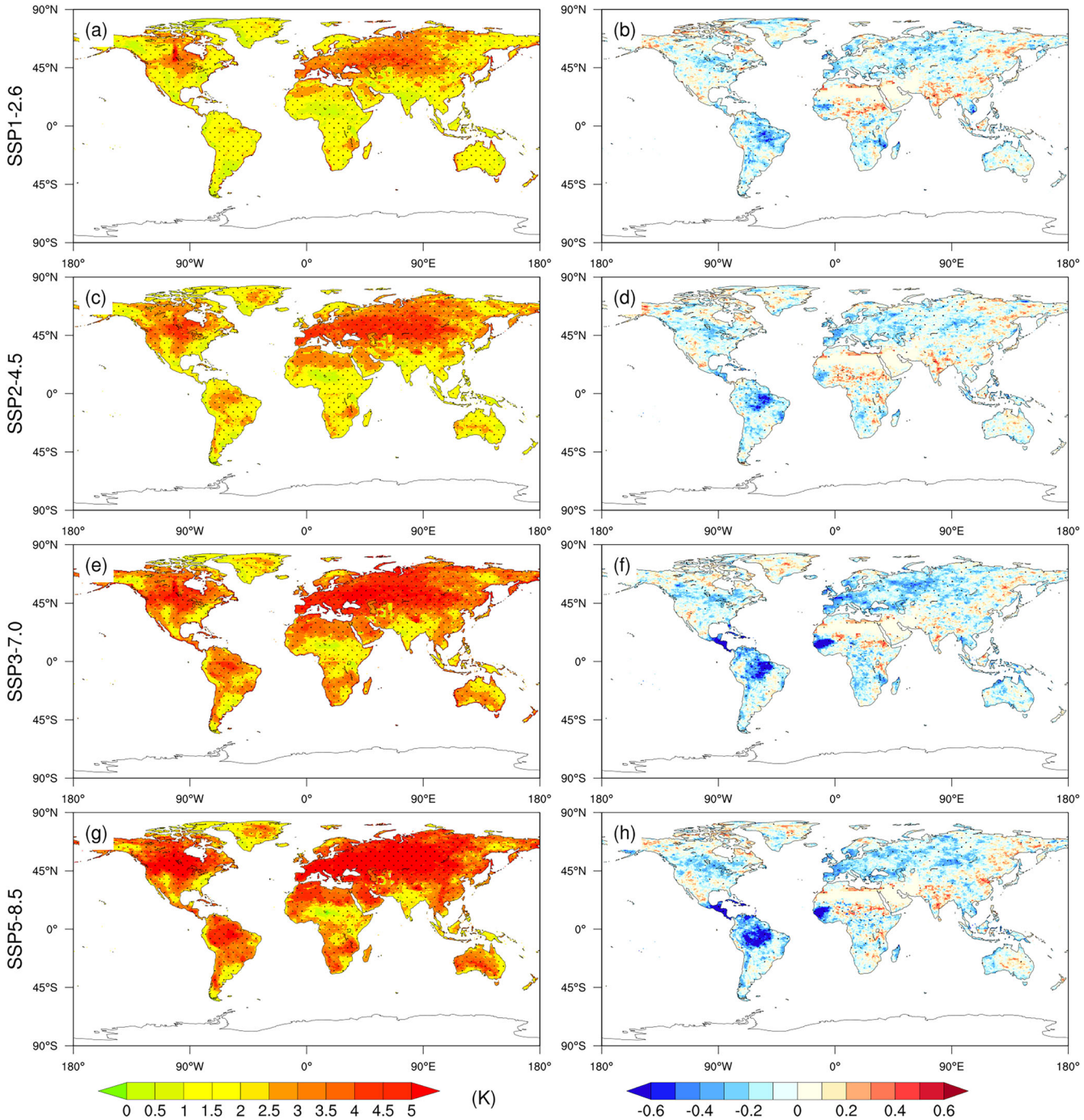

Fig. 2 | Projected changes in hot and dry intensity of hot-dry events under different climate scenarios. Changes in annual mean hot intensity (left column, unit: K) and dry intensity (right column, unitless) are shown for the period 2041–2070 relative to the baseline period (1981–2010): (**a**, **b**) SSP1-2.6, (**c**, **d**) SSP2-4.5, (**e**, **f**) SSP3-7.0, (**g**, **h**) SSP5-8.5. Light gray dots indicate areas where changes are statistically significant at a 5% level based on the Student's *t* test.

displays a general upward trend with increasing emissions. The regions experiencing the most pronounced increase in dryness intensity are primarily concentrated in Europe and Central Asia. In the Southern Hemisphere, areas near the equator, such as northern South America and parts of central Africa, are also expected to become drier relative to the baseline period. Figures S2 and S3 illustrate the uncertainty in model projections of hot-dry event intensity. For hot intensity, higher uncertainty is found in the Northern Hemisphere, particularly under the SSP3-7.0 and SSP5-8.5 scenarios. In contrast, notable uncertainty in dry intensity is expected in central Africa and northern South America, likely due to known challenges in simulating precipitation variability in these regions[34,35].

We investigated the return periods of high-end extreme events under various future scenarios to analyze the probability of occurrence of historically most extreme events in the future. The spatial patterns and regional averages of projected return periods are depicted in Fig. S4 and Table 1. Overall, the return periods of high-end events are projected to decrease in the future, implying that such extreme events will occur more frequently than in the past (i.e., shifting from a 30-year event to one occurring every few years). This increasing risk is evident across all scenarios, with the shortest return periods projected under SSP5-8.5. Spatially, regions including southern South America, most of Africa, the Middle East, Europe, and Central Asia show the most marked reductions in return periods. Among

these, countries in the Middle East and Africa (0.54–1.41 years) and most of Asia (0.74–1.77 years) are projected to experience the highest likelihood of extreme events, while developed regions such as those in the OECD (the Organization for Economic Co-operation and Development 90, EU member states and candidates) show the longest return periods (1.39–2.38 years). The cumulative probability distribution of return periods for high-end extreme events across all global grid points and within subregions can provide an indication of the proportion of grid points falling within specific return periods (Fig. 3) The analysis clearly indicates that under higher emission scenarios, a larger proportion of the globe will experience high-end extreme events with return periods shorter than a defined threshold, particularly evident in the ASIA and MAF regions.

Population exposure to hot-dry extremes

The changes in population exposure to hot-dry compound extremes under the four emission scenarios are influenced by climate change, population dynamics, and their interactions, resulting in distinct spatial patterns (Fig. S5). Population exposure is projected to increase substantially in regions such as Southeast Asia, the Indian subcontinent, and central Africa, compared to the baseline period, while a decrease is expected in the high-latitude regions of the Northern Hemisphere. According to contribution analysis (see Methods section), the climate factor (ΔE_1) plays a dominant role in driving exposure changes compared to other factors. This is primarily because a large population base combined with intensified hot-dry events can significantly elevate exposure levels—even modest climate changes can lead to substantial changes in exposure. On the other hand, the interaction of climate change and population dynamics (ΔE_3) becomes especially influential under the SSP3-7.0 scenario, particularly in the Indian subcontinent and Africa. This is primarily due to the interplay between climate change and population dynamics—such as the increased frequency of extreme events and continued population growth in vulnerable regions—which pronouncedly amplifies population exposure to hot-dry compound extremes[3].

From a regional perspective, the five major economic areas show distinct patterns in future population exposure risks and the relative contributions of different factors (Fig. 4). Overall, the MAF and ASIA regions, with the highest population base among the five regions, would face substantial exposure risks, even under relatively modest increases in the frequency of compound hot-dry extreme events (Fig. 4d, e). Conversely, the REF region (the Reforming Economies of Eastern Europe and the Former Soviet Union) exhibits the lowest exposure risk, mainly due to its relatively small population. Under SSP1-2.6 and SSP5-8.5, anticipated population decline further mitigates this risk, leading to comparatively lower exposure levels (Fig. 4b). Across most regions and scenarios, climate change remains the primary contributor, followed by the interaction between climate and population, and then population alone (Fig. 4f–i). Notably, as emission concentrations increase, the relative contribution of the interaction effect also tends to rise (with SSP5-8.5 possibly being an exception). In most areas, SSP5-8.5 is associated with substantially higher exposure levels, primarily driven by the increased frequency of hot-dry events.

Figure S6 illustrates the uncertainty analysis of changes in population exposure, decomposed into the contributions from climate effects, population effects, and their interaction across different regions and SSP scenarios. The results show that the climate effects constitute the primary source of uncertainty in future exposure projections. Notably, the SSP3-7.0, which assumes a larger population, results in increased uncertainty in regions such as ASIA, MAF, LAM. In contrast, in the OECD region, SSP5-8.5 shows slightly elevated uncertainty, mainly due to the interaction effects between population and climate.

Table 1 | Regional-average return periods (years) for high-end events in the period 2041–2070 across various scenarios

	SSP1-2.6	SSP2-4.5	SSP3-7.0	SSP5-8.5
ASIA	1.77	1.32	0.96	0.74
LAM	1.97	1.58	1.11	0.95
MAF	1.41	1.03	0.72	0.54
OECD	2.38	2.14	1.62	1.39
REF	1.97	1.63	1.35	1.10

Vulnerability in the face of hot-dry events

Socioeconomic disparities. In general, a country's economic condition serves as a key indicator of its resilience and adaptability to natural hazards.

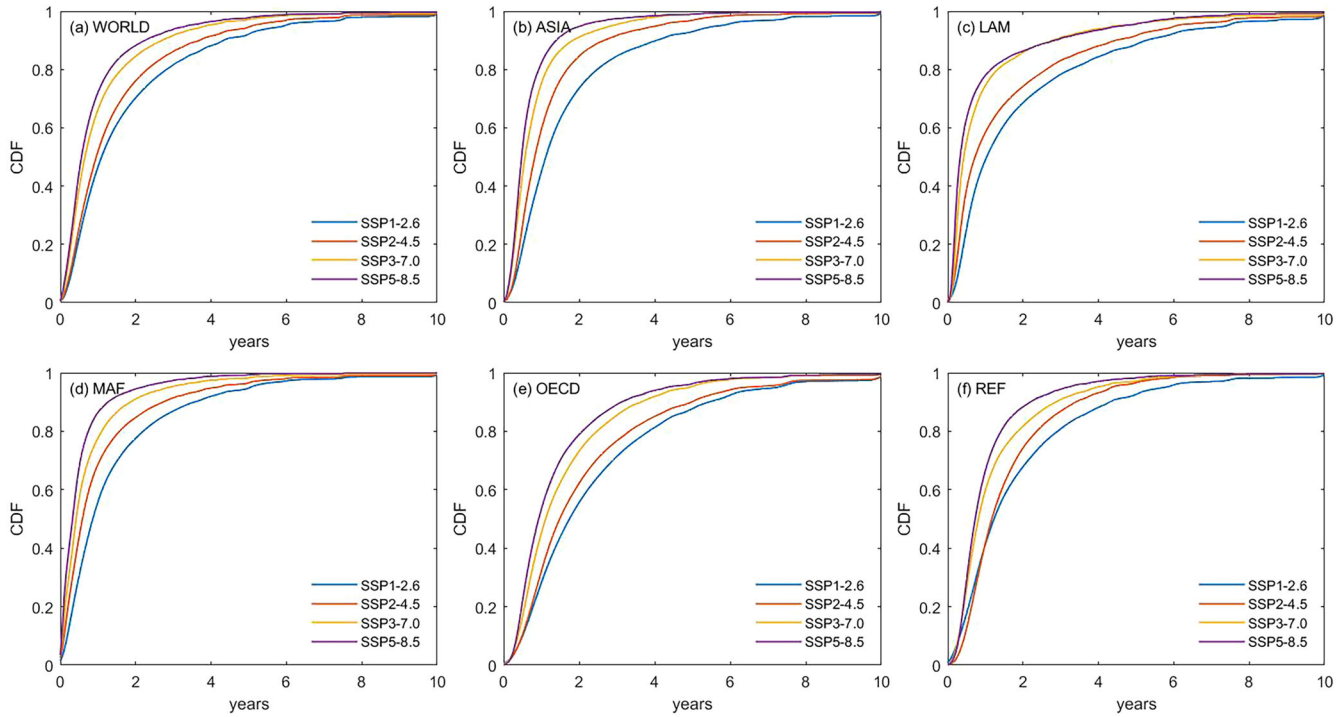

Fig. 3 | Cumulative probability distribution of global and regional return periods for high-end events under different climate scenarios.

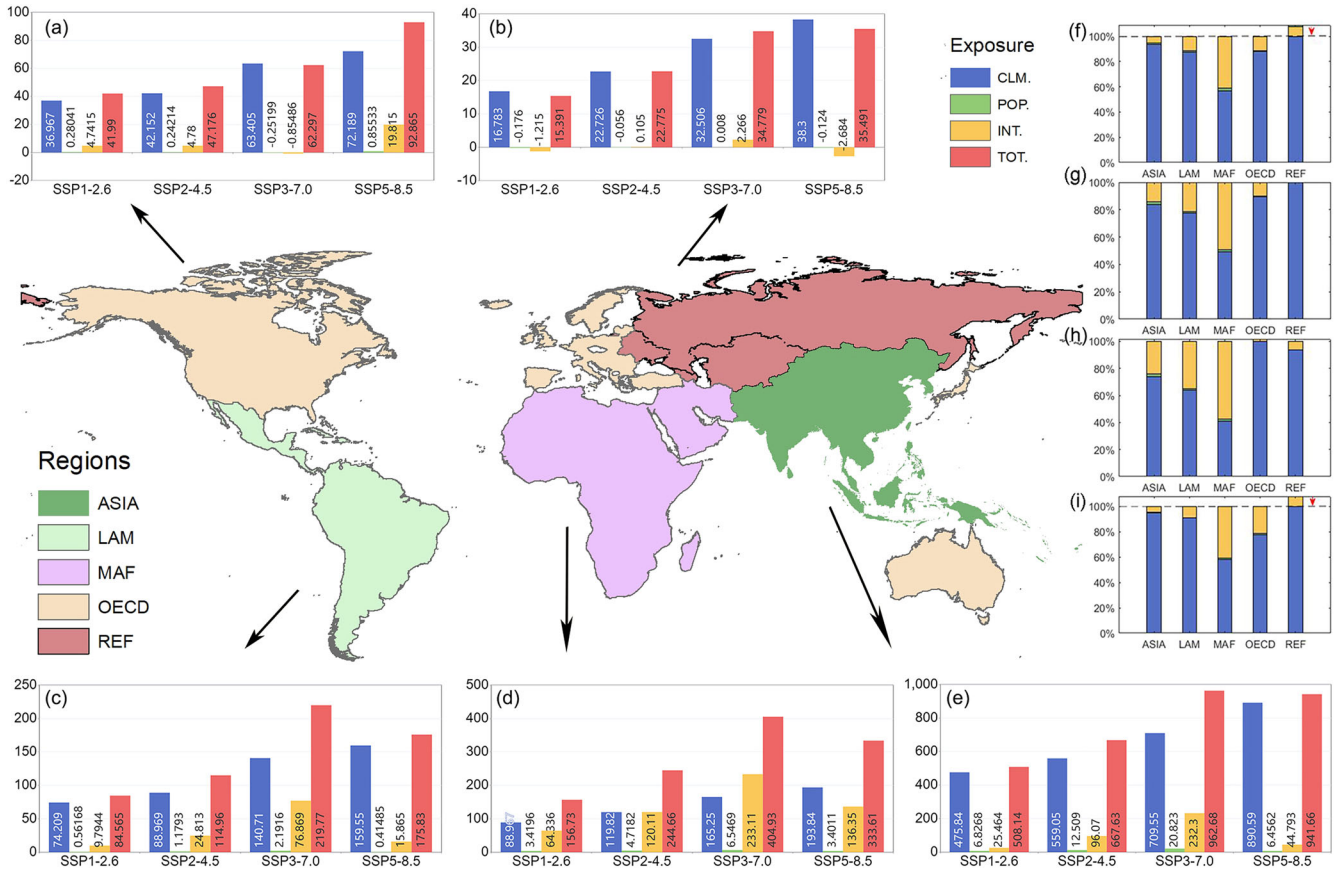

Fig. 4 | Population exposure and contributing factors to hot-dry events across global subregions and scenarios. Changes in population exposure (bar, unit: Kpop×days, where Kpop=thousand people) and relative contributions (stacked bar, unit: %) under different SSP scenarios are shown for: **a** OECD, **b** REF, **c** LAM, **d** MAF, **e** ASIA, **f** SSP1-2.6, **g** SSP2-4.5, **h** SSP3-7.0 and **i** SSP5-8.5.

Economically stronger countries typically possess greater financial resources, well-developed infrastructure, and robust social safety nets, enabling more effective prevention, mitigation, and recovery from hazard-induced losses[36].

Based on the economic classifications of the five major regions (Fig. S7), the OECD region ranks highest, with more than 80% of its population belonging to the high-income category. From a purely economic perspective, although population exposure in the OECD region is at a moderate level relative to other regions (Fig. 4), the associated overall risk is likely to be relatively low due to its stronger economic capacity. Conversely, MAF and ASIA, particularly the former, exhibit both high levels of population exposure and the weakest economic conditions. This combination suggests limited governmental capacity to implement effective adaptation and mitigation strategies, rendering these regions more vulnerable to the increasing frequency of hot-dry compound events in the future.

Leading countries in exposure. Compared to the baseline period, countries in Sub-Saharan Africa, Latin America and the Caribbean, and the Middle East and North Africa are projected to constitute a larger proportion of the top 50 countries with the greatest annual incremental population exposure to hot-dry compound events (Fig. 5). Collectively, these nations may account for over 60% of the total. Notably, low- and lower-middle-income countries constitute a pronouncedly higher proportion of these high-exposure nations compared to other income groups. Under the SSP2-4.5 and SSP3-7.0 scenarios, this proportion could reach ~58%, underscoring the heightened vulnerability of less developed countries to future compound climate extremes. Particularly, populous countries such as India consistently rank among the top 20 in exposure. Countries with high population density are also expected to face greater exposure risks in the future. For instance, Bangladesh, ranked first, has a small land area but a large population, making it one of the most densely populated countries in the world. Additionally, it is worth mentioning that some European countries show a notable increase in both the number of countries (from 5 to 7) and rankings under the SSP5-8.5 scenario, including nations like Italy and the United Kingdom.

Changes in elderly population exposure. In the context of increasing hot-dry compound events, the elderly population emerges as one of the most vulnerable groups. Firstly, seniors typically exhibit relative frailty in terms of their physical and physiological resilience, making them more prone to heat-related illnesses, such as heatstroke, dehydration and cardiovascular complications[37]. Additionally, certain chronic illnesses or underlying health conditions prevalent among the elderly, such as cardiovascular and respiratory diseases, further heighten their sensitivity and risk to heat waves and droughts[38]. We conducted statistical analyses on global population trends, including total and elderly (65+) populations from 2010 to 2070 under different regions and scenarios (Fig. S8). The findings indicate a clear trend of population aging worldwide, with particularly notable implications for the MAF region, where the elderly population may increase by 5–9 times by 2070 compared to the baseline (Table S2).

Regionally, Asia and Africa are projected to remain the most populous continents, especially under the SSP3 "rocky road" scenario, which assumes limited mitigation and adaptation efforts. Under this pathway, population growth is especially pronounced. Regarding the elderly population, Asia exhibits a steep upward trend, particularly under SSP1 and SSP5. OECD countries rank second in terms of elderly population, though their growth is comparatively moderate. Notably, the MAF region, despite having a small elderly base at the century's start, shows the fastest growth rate. By 2070, under SSP1 and SSP5, its elderly population is projected to nearly or even surpass that of OECD countries. Table 2 presents the percentage change in

High income Higher middle income Lower middle income Low income

(a) Leading countries SSP-1.26		(b) Leading countries SSP2-4.5		(c) Leading countries SSP3-7.0		(d) Leading countries SSP5-8.5	
1	BANGLADESH 3953.8	1	BANGLADESH 6259.9	1	BANGLADESH 8802.4	1	BANGLADESH 7055.8
2	HAITI 3377.2	2	JAMAICA 4370	2	EL_SALVADOR 7393.9	2	RWANDA 6184.5
3	JAMAICA 3331.9	3	HAITI 4081.3	3	LEBANON 6655.8	3	LEBANON 5382.7
4	EL_SALVADOR 3277.6	4	RWANDA 4053.6	4	RWANDA 6603.2	4	BURUNDI 4967.5
5	QATAR 3108.7	5	BURUNDI 3640.5	5	JAMAICA 6525.3	5	QATAR 4605.5
6	LEBANON 2575.3	6	QATAR 3438.3	6	HAITI 6190.4	6	ISRAEL 4401.5
7	RWANDA 2340.6	7	EL_SALVADOR 3346.8	7	PHILIPPINES 4759.8	7	HAITI 3609.3
8	PHILIPPINES 2319.1	8	ISRAEL 2872.4	8	ISRAEL 4485.8	8	PHILIPPINES 3528.9
9	ISRAEL 2257.3	9	PHILIPPINES 2826.1	9	DOMINICA 3873.6	9	JAMAICA 3450.4
10	DOMINICA 1931.5	10	PUERTO_RICO 2445.8	10	PUERTO_RICO 3734.4	10	EL_SALVADOR 3323.1
11	PUERTO_RICO 1820.5	11	DOMINICA 2442.1	11	QATAR 3644.5	11	VIETNAM 2768.8
12	BURUNDI 1813.1	12	LEBANON 2427.2	12	EAST_TIMOR 3506.1	12	UNITED_ARAB_EMIRATES 2670.4
13	CYPRUS 1750.8	13	UNITED_ARAB_EMIRATES 1962.3	13	BURUNDI 3372.2	13	DOMINICA 2419.4
14	VIETNAM 1715.4	14	MALAWI 1929	14	GUATEMALA 3343.3	14	MALAWI 2410.9
15	UNITED_ARAB_EMIRATES 1641.2	15	EAST_TIMOR 1777.8	15	SRILANKA 3063.1	15	SRILANKA 2367.3
16	SRILANKA 1516.8	16	SRILANKA 1731.7	16	VIETNAM 2884	16	PUERTO_RICO 2256.8
17	EAST_TIMOR 1344.5	17	VIETNAM 1688.2	17	NIGER 2877.6	17	CYPRUS 2203.6
18	MALAWI 1227.1	18	INDIA 1637.7	18	MALAWI 2810.8	18	INDIA 2189.3
19	COSTA_RICA 1174.5	19	NIGER 1626.9	19	INDIA 2380.9	19	NIGER 2150.7
20	INDIA 1104.9	20	CYPRUS 1416.2	20	UGANDA 2102	20	GUATEMALA 1920.2
21	GUATEMALA 1078.2	21	GUATEMALA 1372.3	21	UNITED_ARAB_EMIRATES 1939.5	21	COSTA_RICA 1536.7
22	NIGER 988.85	22	UGANDA 1057	22	COSTA_RICA 1886.2	22	SIERRA_LEONE 1509.9
23	TRINIDAD_AND_TOBAGO 842.13	23	THAILAND 1009.8	23	CYPRUS 1736.9	23	ITALY 1460.3
24	INDONESIA 839.36	24	NEPAL 971.2	24	SIERRA_LEONE 1668.1	24	JAPAN 1402.6
25	CUBA 815.1	25	GHANA 960.74	25	HONDURAS 1596.3	25	UGANDA 1383
26	JAPAN 807.03	26	INDONESIA 909.68	26	GHANA 1564	26	THAILAND 1370.3
27	THAILAND 751.09	27	SIERRA_LEONE 905.74	27	SYRIAN_ARAB_REPUBLIC 1479.6	27	TRINIDAD_AND_TOBAGO 1285.9
28	UGANDA 695.78	28	COSTA_RICA 904.28	28	INDONESIA 1417	28	JORDAN 1244
29	ITALY 689.5	29	CUBA 900.72	29	THAILAND 1414.3	29	UNITED_KINGDOM 1183.8
30	SIERRA_LEONE 682.01	30	EGYPT 827.45	30	TRINIDAD_AND_TOBAGO 1404.1	30	INDONESIA 1173.7
31	UNITED_KINGDOM 661.61	31	PAKISTAN 793.41	31	NEPAL 1261.7	31	EAST_TIMOR 1147.1
32	NEPAL 647.27	32	JORDAN 781.58	32	IRAQ 1258.3	32	GHANA 1142.2
33	NETHERLANDS 620.05	33	HONDURAS 751.41	33	COTE_DVOIRE 1239.8	33	SYRIAN_ARAB_REPUBLIC 1118.1
34	EGYPT 619.01	34	ITALY 742.46	34	CUBA 1217.8	34	NEPAL 1089.4
35	JORDAN 563.68	35	JAPAN 735.48	35	EGYPT 1213.7	35	EGYPT 1072.8
36	GHANA 548.69	36	IRAQ 709.97	36	PAKISTAN 1172.3	36	NETHERLANDS 1053.8
37	ALBANIA 529.97	37	COTE_DVOIRE 689.51	37	NICARAGUA 1094.1	37	IRAQ 1044.3
38	HONDURAS 526.19	38	SYRIAN_ARAB_REPUBLIC 684.33	38	YEMEN 1052.6	38	HONDURAS 1012.4
39	SYRIAN_ARAB_REPUBLIC 482.14	39	TRINIDAD_AND_TOBAGO 656.11	39	JORDAN 1032	39	PAKISTAN 1000.5
40	FIJI 479.24	40	FIJI 650.53	40	FIJI 1026.1	40	BELGIUM 969.77
41	PAKISTAN 476.59	41	YEMEN 635.66	41	TOGO 973.48	41	CUBA 958.11
42	COTE_DVOIRE 471.39	42	TOGO 617.85	42	BENIN 930.71	42	LIBERIA 891.93
43	NICARAGUA 444.48	43	UNITED_KINGDOM 575.62	43	CAMBODIA 862.99	43	TOGO 889.74
44	BENIN 408.64	44	BENIN 568.61	44	ITALY 860.68	44	COTE_DVOIRE 885.31
45	CAMBODIA 389.8	45	CAMBODIA 559.85	45	ETHIOPIA 816.61	45	BENIN 820.7
46	KUWAIT 384.3	46	NICARAGUA 529.23	46	JAPAN 808.73	46	SWITZERLAND 812.29
47	TOGO 377.79	47	NETHERLANDS 526.71	47	ALBANIA 803.8	47	KUWAIT 746.09
48	IRAQ 374.28	48	ETHIOPIA 512.09	48	LIBERIA 767.55	48	ALBANIA 717.28
49	YEMEN 371.26	49	ALBANIA 509.39	49	NETHERLANDS 740.54	49	MALAYSIA 699.23
50	BELGIUM 368.24	50	LIBERIA 502.8	50	UNITED_KINGDOM 730.82	50	CAMBODIA 690.41

Fig. 5 | Leading 50 countries with the largest projected increase in population exposure to hot-dry compound events. Annual increase in population exposure to hot-dry compound events (unit: Kpop × days, where Kpop = thousand people) are shown for the period 2041–2070 under different SSP scenarios: **a** SSP1-2.6, **b** SSP2-4.5, **c** SSP3-7.0, and **d** SSP5-8.5 scenarios.

Table 2 | Population exposure changes (%) across different scenarios and regions (elderly population exposure changes in parentheses)

	ASIA	LAM	MAF	OECD	REF
SSP1-2.6	501.92 (2457.53)	546.47 (2523.93)	688.84 (2899.95)	292.16 (699.52)	252.21 (798.98)
SSP2-4.5	730.99 (2651.51)	802.72 (2785.89)	1198.47 (3256.33)	372.75 (761.32)	350.52 (805.55)
SSP3-7.0	1115.33 (2945.18)	1365.63 (3447.10)	2043.71 (3849.51)	492.58 (959.51)	570.99 (956.01)
SSP5-8.5	1113.79 (5071.43)	1147.12 (5023.99)	1729.01 (6879.06)	889.42 (1699.76)	616.17 (1721.58)

exposure to hot-dry events for both total and elderly populations under different scenarios. Compared to the baseline period, global population exposure is projected to increase severalfold (ranging from SSP1 to SSP5), with elderly exposure rising even more sharply, increasing by several dozen times in some regions, particularly in MAF. As previously mentioned, Asia and Africa are particularly vulnerable due to their large population bases. In Asia, for instance, the elderly population is expected to grow nearly fivefold, while the duration of hot-dry events could increase by more than sixfold, jointly driving pronounced exposure increases. In Latin America, the sharp rise in exposure risks is primarily driven by the considerable increase in hot-dry events, especially under the SSP3-7.0 and SSP5-8.5 scenarios, potentially resulting in exposure increasing by tens of times. These findings underscore the urgency of focusing adaptive capacity and mitigation efforts in regions with high climate sensitivity and rapidly aging populations.

The contributions of climate change, population aging, and their interaction factors to the exposure of elderly populations to hot-dry extreme events under different scenarios are further examined (Fig. 6). A notable distinction from the drivers of the total population is that the interaction between climate change and population aging accounts for a substantially larger proportion of elderly exposure risk (exceeding 50% in certain regions). Moreover, this interaction effect intensifies under higher emission scenarios. In other words, under different SSP scenarios, the combined

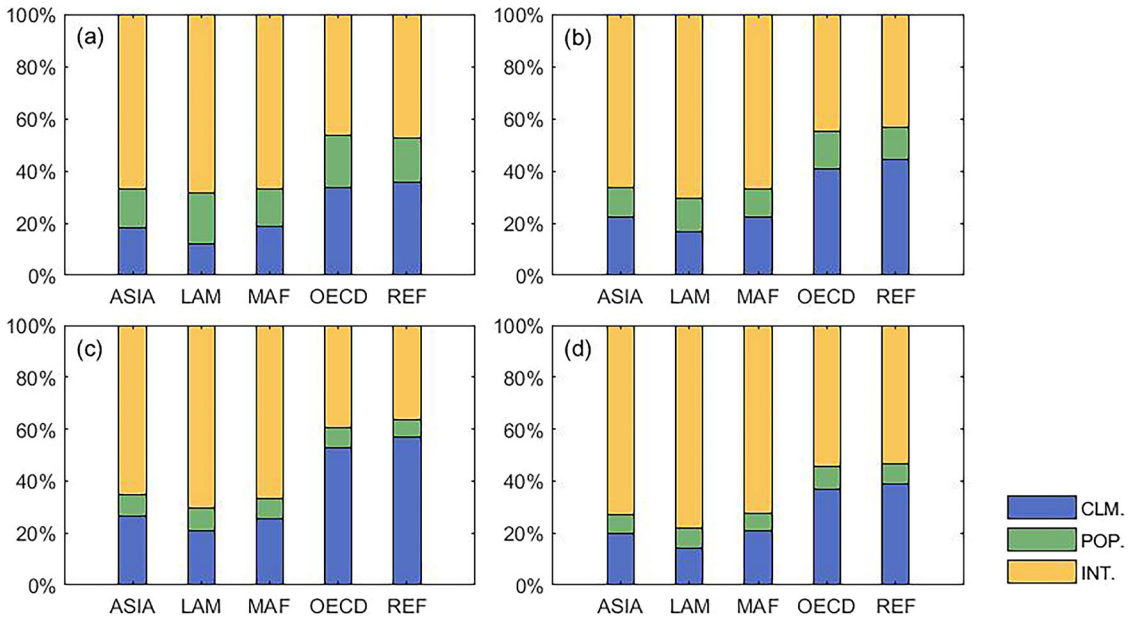

Fig. 6 | Drivers of elderly population exposure to hot-dry compound extremes under different climate scenarios. Relative contributions of climate change, population growth, and their interaction to elderly population exposure across global subregions are shown for the period 2041–2070 under different SSP scenarios: **a** SSP1-2.6, **b** SSP2-4.5, **c** SSP3-7.0, and **d** SSP5-8.5.

impact of climate change and demographic aging becomes increasingly prominent. As population aging accelerates, these regions are projected to face markedly elevated risks of exposure to hot-dry compound extreme events.

Discussion

With the intensification of global warming, compound hot-dry events are projected to increase in frequency, duration, and intensity on a global scale[11,18,20]. The underlying driving mechanisms behind the increasing compound hot-dry events are multifaceted, involving both anthropogenic and natural factors. While precipitation deficits are a fundamental component of drought, human-induced greenhouse gas emissions are a primary contributor to rising surface temperatures, which can intensify the frequency and severity of such compound events. However, the extent to which these changes can be directly attributed to anthropogenic climate change remains under active investigation[19,21]. One key mechanism is the soil moisture–temperature feedback, which amplifies hot-dry conditions through land-atmosphere interactions[39]. A depletion of soil moisture leads, on one hand, to reduced evaporation and, on the other, to enhanced sensible heat fluxes that, ultimately, contribute to the increment of surface air temperatures[8,40,41]. Warmer air, in turn, enhances atmospheric moisture demand, further exacerbating both drying conditions and heat extremes. This self-reinforcing feedback loop plays a central role in sustaining and intensifying hot-dry extremes, often contributing to their persistence and spatial clustering[42,43].

Additionally, from a broader perspective, large-scale atmospheric anomalies (such as El Niño and La Niña events) play a pivotal role in triggering and sustaining hot-dry compound events[10,12,22,44]. The correlation between temperature and soil moisture is intensified due to enhanced land–atmosphere feedbacks and changes in their underlying thermodynamical and dynamical driving mechanisms[20]. Furthermore, other local-scale phenomena driven by human activity (e.g. changes in the land cover[22], urban heat island effect[44,45]) may also contribute to escalation of already established hot and dry anomalies.

Although projections across four emission scenarios indicate an increase in future hot-dry extreme events and associated population exposure, the magnitude of these increases varies among scenarios. Under the SSP1-2.6 scenario, characterized by sustainable development and significant long-term reductions in greenhouse gas emissions, hot-dry extreme events are still expected to rise, but to a much lesser extent compared to SSP5-8.5, which assumes continued high emissions without early mitigation[3]. In contrast, due to the substantial population increase projected under the SSP3 scenario, it is anticipated that population exposure will experience the greatest rise correspondingly. These results are consistent with previous studies, which have similarly identified SSP3 as the scenario with the highest population exposure to diverse hazards[20,46].

In terms of spatial distribution, the overall hot-dry exposure risks are highest in the ASIA and MAF regions, primarily due to their large population bases, which amplify the impacts of climate change. As a result, slight enhancements in hazard risks driven by future climate change could lead to disproportionately severe impacts in these areas[47]. Moreover, both regions are characterized by relatively low income levels, especially in MAF, which exhibits the highest population exposure alongside the poorest economic conditions. This implies that low-income populations may be more exposed or vulnerable to natural hazards than wealthier individuals. Accordingly, climate change impacts vary significantly across income groups[12], underscoring the importance of incorporating socioeconomic disparities and regional complexities into the formulation of climate mitigation policies. Furthermore, the rising population exposure projected in certain developed countries in Latin America and Europe also warrants particular attention in future risk assessments.

With the exacerbation of aging, the elderly will continue to face notable risks from hot-dry compound events. Compared to the baseline, global population exposure is projected to increase severalfold, while exposure among the elderly tends to surge by several dozen times, particularly in Asia and Africa. As aging continues to increase, these regions are expected to face even greater vulnerability to extreme hot-dry disasters[29].

Our study also has several limitations that warrant acknowledgment. Firstly, it is important to recognize the inherent uncertainties associated with data sources. To mitigate these uncertainties, the use of multi-model ensemble is widely recommended for reducing model-specific biases and improving robustness[22]. In this study, we utilized 11 downscaled CMIP6 models to investigate exposure risks to hot-dry extremes under different SSP scenarios. As discussed, there is a certain degree of uncertainty among models regarding future projections for the duration and intensity of hot-dry extremes, population exposure, and contributing factors. Future

research would benefit from incorporating a broader set of CMIP6 models to enhance the representativeness of climate projections. Additionally, a simple arithmetic ensemble mean method is employed to characterize the results, which may inadvertently amplify the weighting of underperforming models[48]. Future efforts should consider applying model ranking or performance-based weighting schemes to improve the credibility of ensemble results and minimize bias from individual models[23,49]. Moreover, uncertainty also arises from future population and economic projections, which are inherently influenced by socioeconomic trajectories. In our analysis, we adopted the World Bank's income-based classification to explore the relationship between economic status and exposure risks across five major regions. However, this classification does not fully account for regional climatic heterogeneity. For example, although Australia shares an income category with North America and Europe, its climate differs substantially. To better inform adaptation planning, future work should explore hybrid regionalization frameworks that integrate both climatic zones and economic tiers. Additionally, utilizing more advanced and high-resolution socioeconomic data (both spatially and temporally) would improve the accuracy of population exposure estimations[23].

Methodological choices introduce another major source of uncertainty. Different definitions and thresholds for hot-dry events can lead to varying estimates of exposure[3,6,23]. Some studies suggest that using precipitation to define dryness yields smaller expected changes compared to definitions based on soil moisture[20]. Thus, using soil moisture instead of precipitation to define dry events may lead to different results. Besides, our study focuses on summer months, which is common practice in studies of mid-latitude extremes[19,50]. However, tropical regions generally lack clear seasonal divisions and are instead dominated by wet and dry seasons. Thus, the conventional definition of "summer" may not adequately capture the spatiotemporal characteristics of tropical climates. Lastly, the calculation of the return period is based on classical extreme value theory[51], which assumes statistical independence among extreme events. This assumption has been widely adopted in many traditional studies as it simplifies computations and provides intuitive estimates of return periods. However, we also recognize that autocorrelation within time series may affect the assumption of independence, especially when calculating hot extreme events based on daily temperature. This could introduce additional uncertainty into return period estimates[52].

Methods

Data

Daily near-surface air temperature and precipitation are obtained from 11 CMIP6-GCMs (Supplementary Table S1) provided by the NASA Earth Exchange Global Daily Downscaled Projections (NEX-GDDP) dataset. The GCM outputs are bias-corrected by employing a statistical downscaling algorithm and are available at 0.25° spatial resolution globally[53]. In this study, we selected the historical baseline period spanning from 1981 to 2010 and conducted future projections for the mid-century period (2041–2070) under four scenarios known as shared socioeconomic pathways and representative concentration pathways (SSPs). These scenarios, namely SSP1-2.6, SSP2-4.5, SSP3-7.0 and SSP5-8.5, integrate the socioeconomic pathways with different climate forcings and represent a sustainable scenario, a medium-growth scenario, a regional rivalry scenario and a fossil-fueled development scenario[54], respectively.

To investigate the impact of hot-dry events on the population, the Global One-Eighth Degree Population Base Year and Projection Grids Based on the SSPs dataset (v1.01) is utilized[6,55]. This dataset includes total population data for the base year and population projections at 10-year intervals from 2010–2100 at a 0.125° spatial resolution, allowing it to effectively reflect the population dynamics described in each SSP narrative[56]. This alignment makes it a valuable tool frequently employed to evaluate climate change vulnerability, impacts, and adaptation. It should be noted that given the global population grid data used in this study has a different temporal resolution from the continuous hot-dry data, the population exposure is calculated as follows: the population data from 2010 was used as the baseline period. For future periods, exposure is calculated using the average population values for the years 2040, 2050, 2060, and 2070, which corresponds to the average hot-dry period of 2041–2070.

Supplementing the dataset, data on the elderly population (65+) from historical periods and various SSP scenarios are essential for evaluating the risks and challenges posed by aging populations when confronted with compounded impacts of hot-dry events in diverse global regions. The data on the aged population originate from the SSP database, developed by the International Institute for Applied Systems Analysis (IIASA)[54]. Since these data are available at the national scale rather than at the grid level, we first compute the mean of compound hot-dry events across all grid cells within each country, thereby generating country-aggregated indices. Subsequently, the exposure of the elderly population to these events can be calculated at the national or regional scale.

In examining the vulnerability of populations to exposure risks during hot-dry compound events, the level of economic development is a pivotal factor under consideration. In this study, we followed IIASA's classification to divide the world into five major economic regions, which are delineated as follows[57]: OECD (the Organization for Economic Co-operation and Development 90, EU member states and candidates), REF (the Reforming Economies of Eastern Europe and the Former Soviet Union), ASIA (most Asian countries except for the Middle East, Japan and Former Soviet Union states), MAF (countries of the Middle East and Africa), LAM (countries of Latin America and the Caribbean). Additionally, according to the classification standards set by the World Bank Group, based on current GDP, we categorized countries worldwide into four income groups: low-income, lower-middle-income, upper-middle-income, and high-income (Fig. S7). The World Bank's classifications are dynamic and undergo annual updates as of July 1st, primarily relying on the previous year's per capita Gross National Income (in US dollars)[58]. To evaluate population exposure based on income levels, we averaged the hot-dry climate grid data at the country and regional levels. Then, the risk of population exposure across different regions and countries with varying income levels was analyzed.

hot-dry event definition

A hot-dry event is defined as a period with co-occurring heatwave and drought conditions. This study focuses exclusively on compound dry and hot events during the warm season, particularly during the summer months from June to August in the Northern Hemisphere and December to February in the Southern Hemisphere[19,50]. Specifically, we followed these steps to define and identify a hot-dry extreme event (Fig. S9).

Data sample. The maximum daytime and minimum nighttime temperatures, along with daily precipitation data for the summer season (June-August for the Northern Hemisphere and December–February for the Southern Hemisphere), are first extracted to construct the sample data.

Heatwave identification. For each grid, a hot day (or night) in each grid is defined as one where the daily maximum (or minimum) temperature exceeds the 90th percentile threshold, which is calculated for each day of the summer period. To mitigate the influence of the annual cycle and reduce inconsistencies in percentile-based extreme indices, the data for each day are ranked within a 15-day window centered on that day during the baseline period. Then a heatwave event is identified when both the daytime maximum and nighttime minimum temperatures exceed their respective thresholds for three consecutive days in the same grid[43].

Drought identification. The SPI index is chosen to identify drought events. The index is derived by transforming the precipitation time series into a standardized normal distribution, which represents the number of standard deviations by which the observed precipitation anomaly deviates from the long-term mean. The SPI index has been recommended by the WMO as the indicator to track the meteorological drought[18,42,59].

Here, SPI is calculated on a three-month timescale and a meteorological drought event is defined as having an SPI value less than −1, in accordance with WMO's definition[60].

Compound event identification. Years in which both heatwave and drought occur simultaneously are considered instances of hot-dry compound extreme events. The annual duration and intensity of compound hot–dry conditions are calculated as follows:

$$D = \sum_{i=1}^{N} d_i \tag{1}$$

$$I_T = \frac{\sum_{i=1}^{N} \frac{\sum_{j=1}^{d_i} (Tx_{i,j} - TXR_j) + (Tn_{i,j} - TNR_j)}{d_i}}{N} \tag{2}$$

$$I_P = SPI \tag{3}$$

where D is the yearly total number of participating hot-dry extreme days, N is the number of hot-dry extreme events in a given year, i is the index of a hot-dry event. The hot-dry intensity is divided into two components: one is hot intensity (I_T, as defined by Formula 2), where j denotes the day within the hot-dry event (i). Here, d_i is the duration of a hot-dry event (i); $Tx_{i,j}$ and $Tn_{i,j}$ are the daily maximum and minimum temperature at day j during the hot-dry extreme event (i); TXR_j and TNR_j are the 90th percentile thresholds for the daily maximum and minimum temperature at day j. The other component is represented by drought intensity (I_P), which is characterized by the annual average SPI value during hot-dry event years. A lower SPI indicates greater drought intensity. These calculations are performed separately for each GCM, and the ensemble mean is then computed. The statistical significance of future changes in hot-dry extremes at each grid point is assessed using a Student's t test at the 95% confidence level.

Exposure to hot-dry events

The definition of exposure is the presence of people, infrastructure, and other assets in areas where hazardous events may occur[61]. Here, we used the annual population exposure (E) to measure the impact of hot-dry extreme events on the population. Following references[9,23], the E can be indicated as the number of hot-dry events multiplied by the number of people exposed, as follows:

$$E = D \times P \tag{4}$$

where D and P represent the duration of hot-dry events and population in a certain period. The future change in population exposure is calculated as follows:

$$\begin{aligned} \Delta E &= D_f \times P_f - D_h \times P_h = (D_h + \Delta D) \times (P_h + \Delta P) - D_h \times P_h \\ &= \overbrace{\Delta D \times P_h}^{\Delta E_1} + \overbrace{\Delta P \times D_h}^{\Delta E_2} + \overbrace{\Delta D \times \Delta P}^{\Delta E_3} \end{aligned} \tag{5}$$

where ΔE indicates the change in future population exposure compared to the historical period.D_h (D_f) and P_h (P_f) are the number of compound extreme days and population in the historical (future) period, respectively. ΔD and ΔP represent the difference in compound hot–dry extreme days and population between the future and historical periods, respectively.

According to Eq. 5, the future changes in population exposure can be decomposed into three components, namely$\Delta D \times P_h$ (ΔE_1), $\Delta P \times D_h$ (ΔE_2) and $\Delta D \times \Delta P$ (ΔE_3), and they represent the climate effect, population effect and interaction effect on total exposure change. Correspondingly, the relative contribution (%) of climate (RC_{clim}), population (RC_{pop}) and the interaction effect (RC_{inter}) to the total exposure change are calculated as[3,23]:

$$RC_{clim} = \frac{P_h \times \Delta D}{\Delta E} \times 100 \tag{6}$$

$$RC_{pop} = \frac{\mathrm{D}_h \times \Delta P}{\Delta E} \times 100 \tag{7}$$

$$RC_{inter} = \frac{\Delta P \times \Delta D}{\Delta E} \times 100 \tag{8}$$

Return period of the high-end risk

The term "high-end risk" refers to the maximum intensity thresholds of hot and dry events observed during the recent historical period. This analysis aims to assess the likelihood that these events will be equally or more severe in the future than observed in the recent period[26,62]. Essentially, evaluating high-end risk involves estimating the probability of such extreme events occurring in the future or, equivalently, calculating their return period, which is the inverse of the occurrence probability. Specifically, the joint probability of occurrence of high-end risk events for each latitude and longitude grid in the future climate scenario was computed. This probability is obtained by dividing the total number of compound hot-dry days by the overall number of days within that specific period, given as:

$$\begin{aligned} &\mathrm{P}(H \cap D | I_{T,f} \geq I_{T,h}, -SPI_f \geq -SPI_h)_{SSP,lat,lon} \\ &= \frac{\sum_{n=1}^{N} \sum HDE(lat,\ lon,\ SSP | I_{T,f} \geq I_{T,h}, -SPI_f \geq -SPI_h)}{\mathrm{ndays} \times \mathrm{N}} \end{aligned} \tag{9}$$

Where $\mathrm{P}(H \cap D | I_{T,f} \geq I_{T,h}, -SPI_f \geq -SPI_h)_{SSP,lat,lon}$ is the conditional joint probability, $I_{T,h}$ and SPI_h are the maximum hot and dry intensity in the historical period for each grid. Analogously, $I_{T,f}$ and SPI_f are the hot and dry intensity in the future climate scenario (SSP) for each grid, and N is the total number of CMIP6-GCMs used in the study. Subsequently, the return period is computed by normalizing the reciprocal of the conditional probability with the number of days per year. A smaller return period implies a greater risk of future hot-dry events surpassing the intensity observed in historical extremes.

$$RP_{SSP,lat,lon} = \frac{1}{\mathrm{P}(H \cap D | I_{T,f} \geq I_{T,h}, -SPI_f \geq -SPI_h)_{SSP,lat,lon}} \times 365 \tag{10}$$

Data availability

Data analyzed during the current study is the NASA Earth Exchange Global Daily Downscaled Projections (NEX-GDDP-CMIP6) gridded dataset distributed data archive [https://ds.nccs.nasa.gov/].

Received: 25 September 2024; Accepted: 1 July 2025;
Published online: 18 July 2025

References

1. Kong, Q., Guerreiro, S. B., Blenkinsop, S., Li, X.-F. & Fowler, H. J. Increases in summertime concurrent drought and heatwave in Eastern China. *Weather Clim. Extremes* **28**, 100242 (2020).
2. Tang, Y., Luo, M., Wu, S. & Li, X. Increasing synchrony of extreme heat and precipitation events under climate warming. *Geophys. Res. Lett.* **52**, e2024GL113021 (2025).
3. Zhang, G. et al. Climate change determines future population exposure to summertime compound dry and hot events. *Earth's. Future* **10**, e2022EF003015 (2022).
4. Zhang, Y., Hao, Z. & Zhang, Y. Agricultural risk assessment of compound dry and hot events in China. *Agric. Water Manag.* **277**, 108128 (2023).

5. Heino, M. et al. Increased probability of hot and dry weather extremes during the growing season threatens global crop yields. *Sci. Rep.* **13**, 3583 (2023).
6. Liu, W. et al. Increasing population exposure to global warm-season concurrent dry and hot extremes under different warming levels. *Environ. Res. Lett.* **16**, 094002 (2021).
7. Abatzoglou, J. T., Williams, A. P. & Barbero, R. Global emergence of anthropogenic climate change in fire weather indices. *Geophys. Res. Lett.* **46**, 326–336 (2019).
8. Fan, X. et al. Escalating hot-dry extremes amplify compound fire weather risk. *Earth's. Future* **11**, e2023EF003976 (2023).
9. Feng, Y. et al. Changes in compound hot and dry day and population exposure across China under climate change. *Int. J. Climatol*. **42** (2021).
10. Mishra, V., Thirumalai, K., Singh, D. & Aadhar, S. Future exacerbation of hot and dry summer monsoon extremes in India. *npj Clim. Atmos. Sci.* **3**, 10 (2020).
11. Wu, X. et al. Projected increase in compound dry and hot events over global land areas. *Int. J. Climatol.* **41**, 393–403 (2021).
12. Yin, J. et al. Future socio-ecosystem productivity threatened by compound drought–heatwave events. *Nat. Sustain.* **6**, 259–272 (2023).
13. Bian, Y., Sun, P., Zhang, Q., Luo, M. & Liu, R. Amplification of non-stationary drought to heatwave duration and intensity in eastern China: Spatiotemporal pattern and causes. *J. Hydrol.* **612**, 128154 (2022).
14. Luo, M. et al. Observed heatwave changes in arid northwest China: physical mechanism and long-term trend. *Atmos. Res.* **242**, 105009 (2020).
15. Wang, J., Feng, J., Yan, Z. & Chen, Y. Future risks of unprecedented compound heat waves over three vast urban agglomerations in China. *Earth's. Future* **8**, e2020EF001716 (2020).
16. Hao, Z., AghaKouchak, A. & Phillips, T. J. Changes in concurrent monthly precipitation and temperature extremes. *Environ. Res. Lett.* **8**, 034014 (2013).
17. Yin, C. et al. Global near real-time daily apparent temperature and heat wave dataset. *Geosci. Data J.* **10**, 231–245 (2023).
18. Shi, Z., Jia, G., Zhou, Y., Xu, X. & Jiang, Y. Amplified intensity and duration of heatwaves by concurrent droughts in China. *Atmos. Res.* **261**, 105743 (2021).
19. Singh, J. et al. Enhanced risk of concurrent regional droughts with increased ENSO variability and warming. *Nat. Clim. Change* **12**, 163–170 (2022).
20. Tabari, H. & Willems, P. Global risk assessment of compound hot-dry events in the context of future climate change and socioeconomic factors. *npj Clim. Atmos. Sci.* **6**, 74 (2023).
21. Wu, X., Hao, Z., Zhang, X., Li, C. & Hao, F. Evaluation of severity changes of compound dry and hot events in China based on a multivariate multi-index approach. *J. Hydrol.* **583**, 124580 (2020).
22. Zhang, H., Wu, C., Yeh, P. J.-F. & Hu, B. X. Global pattern of short-term concurrent hot and dry extremes and its relationship to large-scale climate indices. *Int. J. Climatol.* **40**, 5906–5924 (2020).
23. Zhao, C. et al. Projected changes in socioeconomic exposure to compound hot–dry/hot–wet days in China under CMIP6 forcing scenarios. *Theor. Appl. Climatol.* **154**, 601–612 (2023).
24. Wu, Y. et al. Global observations and CMIP6 simulations of compound extremes of monthly temperature and precipitation. *GeoHealth* **5**, e2021GH000390 (2021).
25. Dutta, R., Chanda, K. & Maity, R. Future of solar energy potential in a changing climate across the world: a CMIP6 multi-model ensemble analysis. *Renew. Energy* **188**, 819–829 (2022).
26. Tripathy, K. P., Mukherjee, S., Mishra, A. K., Mann, M. E. & Williams, A. P. Climate change will accelerate the high-end risk of compound drought and heatwave events. *Proc. Natl. Acad. Sci. USA* **120**, e2219825120 (2023).
27. De Luca, P. & Donat, M. G. Projected changes in hot, dry, and compound hot-dry extremes over global land regions. *Geophys. Res. Lett.* **50**, e2022GL102493 (2023).
28. Qian, C., Ye, Y., Bevacqua, E. & Zscheischler, J. Human influences on spatially compounding flooding and heatwave events in China and future increasing risks. *Weather Clim. Extremes* **42**, 100616 (2023).
29. Falchetta, G., De Cian, E., Sue Wing, I. & Carr, D. Global projections of heat exposure of older adults. *Nat. Commun.* **15**, 3678 (2024).
30. Chen, M. et al. Rising vulnerability of compound risk inequality to ageing and extreme heatwave exposure in global cities. *npj Urban Sustain.* **3**, 38 (2023).
31. Lafferty, D. C. & Sriver, R. L. Downscaling and bias-correction contribute considerable uncertainty to local climate projections in CMIP6. *npj Clim. Atmos. Sci.* **6**, 158 (2023).
32. Lennard, C. J., Nikulin, G., Dosio, A. & Moufouma-Okia, W. On the need for regional climate information over Africa under varying levels of global warming. *Environ. Res. Lett.* **13**, 060401 (2018).
33. Chen, J., Arsenault, R., Brissette, F. P. & Zhang, S. Climate change impact studies: should we bias correct climate model outputs or post-process impact model outputs?. *Water Resour. Res.* **57**, e2020WR028638 (2021).
34. Komelo, C. K. et al. Evaluation of extreme precipitation events as simulated by CMIP6 models over Central Africa: spatial patterns. *Theor. Appl. Climatol.* **155**, 9579–9599 (2024).
35. Kahana, R., Halladay, K., Alves, L. M., Chadwick, R. & Hartley, A. J. Future precipitation projections for Brazil and tropical South America from a convection-permitting climate simulation. *Front. Clim.* **6** (2024).
36. International Monetary Fund. Western Hemisphere Dept. Economic Benefits of Building Resilience to Natural Hazards and Climate Change. *IMF Staff Country Rep.* **2024**, A002 (2024).
37. Kenney, W. L., Craighead, D. H. & Alexander, L. M. Heat waves, aging, and human cardiovascular health. *Med. Sci. Sports Exerc.* **46**, 1891–1899 (2014).
38. Yang, J. et al. Projecting heat-related excess mortality under climate change scenarios in China. *Nat. Commun.* **12**, 1039 (2021).
39. Miralles, D. G., Gentine, P., Seneviratne, S. I. & Teuling, A. J. Land–atmospheric feedbacks during droughts and heatwaves: state of the science and current challenges. *Ann. N. Y. Acad. Sci.* **1436**, 19–35 (2019).
40. Humphrey, V. et al. Soil moisture–atmosphere feedback dominates land carbon uptake variability. *Nature* **592**, 65–69 (2021).
41. Aminzadeh, M., Roderick, M. L. & Or, D. Using the complementary relationship between actual and potential evaporation to diagnose the onset of heatwaves. *Water Resour. Res.* **57**, e2020WR029156 (2021).
42. Feng, Y. et al. Changes in compound hot and dry day and population exposure across China under climate change. *Int. J. Climatol.* **42**, 2935–2949 (2022).
43. Ma, F. & Yuan, X. More Persistent Summer Compound Hot Extremes Caused by Global Urbanization. *Geophys. Res. Lett.* **48**, e2021GL093721 (2021).
44. Xiang, J., Bi, P., Pisaniello, D. & Hansen, A. Health impacts of workplace heat exposure: an epidemiological review. *Ind. Health* **52**, 91–101 (2014).
45. Luo, M. & Lau, N.-C. Increasing Human-Perceived Heat Stress Risks Exacerbated by Urbanization in China: A Comparative Study Based on Multiple Metrics. *Earth's. Future* **9**, e2020EF001848 (2021).
46. Li, B. et al. Future global population exposure to record-breaking climate extremes. *Earth's. Future* **11**, e2023EF003786 (2023).
47. Chen, H. & Sun, J. Significant increase of the global population exposure to increased precipitation extremes in the future. *Earth's. Future* **9**, e2020EF001941 (2021).
48. Tokarska, K. B. et al. Past warming trend constrains future warming in CMIP6 models. *Sci. Adv.* **6**, eaaz9549 (2020).
49. Guo, J. et al. Picturing China's photovoltaic energy future: insights from CMIP6 climate projections. *Renew. Sustain. Energy Rev.* **189**, 114026 (2024).

50. Zhang, W., Furtado, K., Zhou, T., Wu, P. & Chen, X. Constraining extreme precipitation projections using past precipitation variability. *Nat. Commun.* **13**, 6319 (2022).
51. Omey, E., Mallor, F. & Nualart, E. An introduction to statistical modelling of extreme values. Application to calculate extreme wind speeds. Working Papers 2009/36, Hogeschool-Universiteit Brussel, Faculteit Economie en Management (2009).
52. Li, L. & Yang, C. Percentile-Based ETCCDI Temperature Extremes Indices for CMIP5 Model Output: New Results through Semiparametric Quantile Regression Approach. *AGU Fall Meeting Abstracts*. GC13D-0807 (2017).
53. Thrasher, B. et al. NASA global daily downscaled projections, CMIP6. *Sci. Data* **9**, 262 (2022).
54. Kc, S. & Lutz, W. The human core of the shared socioeconomic pathways: Population scenarios by age, sex and level of education for all countries to 2100. *Glob. Environ. Change* **42**, 181–192 (2017).
55. Jones, B. & O'Neill, B. C. Spatially explicit global population scenarios consistent with the shared socioeconomic pathways. *Environ. Res. Lett.* **11**, 084003 (2016).
56. Jones, B. & O'Neill, B. C. (NASA Socioeconomic Data and Applications Center (SEDAC), Palisades, New York, 2020).
57. Riahi, K. et al. The shared socioeconomic pathways and their energy, land use, and greenhouse gas emissions implications: an overview. *Glob. Environ. Change* **42**, 153–168 (2017).
58. Groups, W. B. C. a. L. *World Bank Income Classifications FY24*, https://blogs.worldbank.org/opendata/new-world-bank-group-country-classifications-income-level-fy24 (2024).
59. Hosseinzadehtalaei, P., Termonia, P. & Tabari, H. Projected changes in compound hot-dry events depend on the dry indicator considered. *Commun. Earth Environ.* **5**, 220 (2024).
60. Svoboda, M., M. H. a. D. Standardized precipitation index user guide. In *WMO-No. 1090, Wood World Meteorological Organization*, *Geneva* (2012).
61. Reduction, U. N. O. f. D. R. Living with risk: a global review of disaster reduction initiatives. https://www.undrr.org/publication/living-risk-global-review-disaster-reduction-initiatives, 429 p (2004).
62. Ridder, N. N. et al. Global hotspots for the occurrence of compound events. *Nat. Commun.* **11**, 5956 (2020).

Acknowledgements

This paper is supported by the Academy of Medical Sciences, British Academy, Royal Academy of Engineering, Royal Society and the International Science Partnerships Fund (NGR2\1867).

Author contributions

Writing-review and editing: J.G., F.W., Y.F., and C.S. Experimental operation: Y.F., J.G., F.W., X.W., Y.W. Data acquisition and validation: H.Z. and Z.H. All authors reviewed the manuscript.

Competing interests

The authors declare no competing interests.

Additional information

Supplementary information The online version contains supplementary material available at https://doi.org/10.1038/s44304-025-00119-x.

Correspondence and requests for materials should be addressed to Yurui Fan or Chunming Shen.